EUROPEAN ORGANIZATION FOR NUCLEAR RESEARCH
CERN – ACCELERATORS AND TECHNOLOGY SECTOR

CERN-ATS-2013-14

RF Plasma modeling of the Linac4 H− ion source

S. Mattei*, M. Ohta†, A. Hatayama†, J. Lettry*, Y. Kawamura†,
M. Yasumoto† and C. Schmitzer*,**

*CERN, 1211 Geneva 23, Switzerland
†Graduate school of Science and Technology, Keio University, 3-14-1 Hiyoshi, Kouhoku-ku, Yokohama 223-8522, Japan
**Technische Universität Wien, 1040 Wien, Karlsplatz 13, Austria

This study focuses on the modelling of the ICP RF-plasma in the Linac4 H− ion source currently being constructed at CERN. A self-consistent model of the plasma dynamics with the RF electromagnetic field has been developed by a PIC-MCC method. In this paper, the model is applied to the analysis of a low density plasma discharge initiation, with particular interest on the effect of the external magnetic field on the plasma properties, such as wall loss, electron density and electron energy. The use of a multi-cusp magnetic field effectively limits the wall losses, particularly in the radial direction. Preliminary results however indicate that a reduced heating efficiency results in such a configuration. The effect is possibly due to trapping of electrons in the multi-cusp magnetic field, preventing their continuous acceleration in the azimuthal direction.

CERN-ATS-2013-014
25/01/2013

Presented at (NIBS 2012), 3.-7. September 2012, Jyväskylä, Finland

RF Plasma modeling of the Linac4 H^- ion source

S. Mattei[*], M. Ohta[†], A. Hatayama[†], J. Lettry[*], Y. Kawamura[†], M. Yasumoto[†] and C. Schmitzer[*,**]

[*]*CERN, 1211 Geneva 23, Switzerland*
[†]*Graduate school of Science and Technology, Keio University, 3-14-1 Hiyoshi, Kouhoku-ku, Yokohama 223-8522, Japan*
[**]*Technische Universität Wien, 1040 Wien, Karlsplatz 13, Austria*

Abstract. This study focuses on the modelling of the ICP RF-plasma in the Linac4 H^- ion source currently being constructed at CERN. A self-consistent model of the plasma dynamics with the RF electromagnetic field has been developed by a PIC-MCC method. In this paper, the model is applied to the analysis of a low density plasma discharge initiation, with particular interest on the effect of the external magnetic field on the plasma properties, such as wall loss, electron density and electron energy. The use of a multi-cusp magnetic field effectively limits the wall losses, particularly in the radial direction. Preliminary results however indicate that a reduced heating efficiency results in such a configuration. The effect is possibly due to trapping of electrons in the multi-cusp magnetic field, preventing their continuous acceleration in the azimuthal direction.

Keywords: Plasma simulation; RF negative ion source; Particle-in-cell; Monte Carlo method
PACS: 52.65.-y; 52.65.Rr; 07.77.Ka

1. INTRODUCTION

To improve beam brightness and luminosity, CERN has launched an upgrade of its injector complex for the Large Hadron Collider (LHC). The present 50 MeV proton injector Linac2 will be replaced by a 160 MeV H^- linear accelerator, Linac4, as the injector to the Proton Synchrotron Booster [1].

The specifications of the Linac4 ion source are to deliver 80 mA of H^- current in pulses of 500 μs within a normalized emittance of 0.25 mm mrad RMS and a repetition rate up to 2 Hz. Three types of ion source are foreseen. The first one, IS-01, is a DESY inspired volume production, pulsed RF-source. IS-01 has been recently constructed and aims at a 20 mA H^- current [2]. To increase the current to 40 mA and to minimize the co-extracted electron current, the IS-02 design is inspired by the SNS cesiated, surface production ion source. To reach the 80 mA current, investigations to operate a magnetron ion source with low repetition rate are currently ongoing.

Both IS-01 and IS-02 are pulsed RF sources, in which the plasma is generated by an external solenoid antenna mounted on the plasma chamber. To optimally design and operate an ion source for volume and surface H^- production, a thorough understanding of the plasma formation and composition is required. Important parameters both in the geometry (e.g. plasma chamber dimensions, coil position and size) and in the operation (eg. coil current, frequency and pressure) are of paramount importance to define the optimum conditions.

The goal of this study is to obtain first insights into RF plasma heating in the Linac4

ion source. The preliminary results from an electromagnetic Particle In Cell, Monte Carlo Collision method (PIC-MCC) on a simplified geometry model and in a low plasma density regime are presented. These first insights into the plasma characteristics allow assessment of the effort required, in terms of code development, to simulate the real Linac4 source conditions.

2. LINAC4 VOLUME ION SOURCE

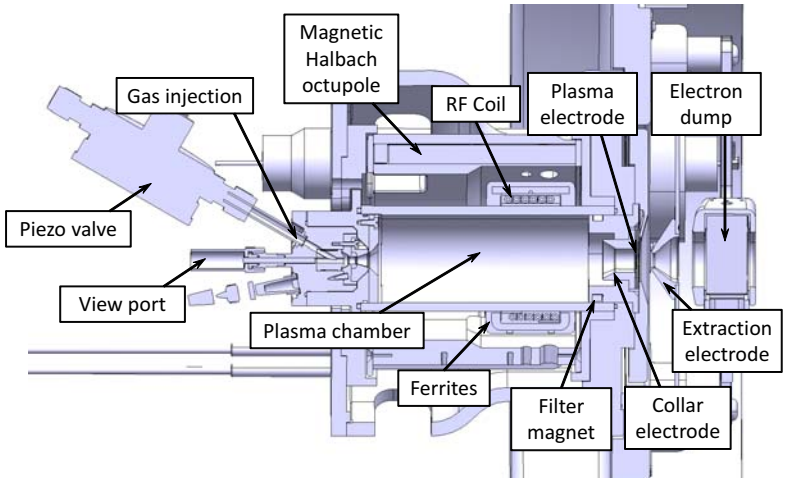

FIGURE 1. Cross section of the IS-01 plasma generator, gas injection and extraction system

A detailed view of the IS-01 ion source is shown in Fig. 1. The 48 mm inner diameter Al_2O_3 plasma chamber is surrounded by a 6 turn solenoid antenna equipped with 6 ferrites. A multi-cusp magnetic field (external permanent magnet octupole in an offset Halbach configuration) surrounds the chamber. A magnetic filter field of 20 mT on the axis, is located between the RF plasma chamber and the beam extraction region. Two electrodes at the source outlet (collar and plasma electrode) can be independently biased. Hydrogen is pulsed into the plasma chamber by means of a piezo valve. The RF power is supplied at 2 ± 0.2 MHz with an available peak power of 100 kW.

3. PIC-MCC CODE DESCRIPTION

We use the model developed in references [3, 4]. The model is based on a PIC-MCC method which consists of two parts. One is the 2D model of the RF electromagnetic field, in which Maxwell's equations are solved by the Finite-Difference Time-Domain (FDTD) method [5]. The other one is the 3D3V particle dynamics model, where the equations of motion of charged particles are solved numerically. Collisions are taken into account by a Monte Carlo method. The model has been extended and applied to the analysis of the Linac4 H^- source.

2D Electromagnetic Model - The free space RF electromagnetic field in the plasma chamber is described by the following Maxwell equations:

$$\nabla \times \mathbf{E} = -\frac{\partial \mathbf{B}}{\partial t} \tag{1}$$

$$\nabla \times \mathbf{B} = \mu_0 \mathbf{j} + \mu_0 \varepsilon_0 \frac{\partial \mathbf{E}}{\partial t} \tag{2}$$

where **E** and **B** are the electric field and the magnetic field vectors, respectively. When the multi-cusp magnetic field is included, $\mathbf{B} = \mathbf{B}_{RF} + \mathbf{B}_{cusp}$ where $\mathbf{B}_{RF}$ is the magnetic field generated by the RF current and $\mathbf{B}_{cusp}$ the multi-cusp magnetic field. The current density **j** consists of two contributions, the RF-coil current $\mathbf{j}_{RFcoil}$ and the plasma current $\mathbf{j}_{plasma}$. Equations (1), (2) are solved by the FDTD method in cylindrical coordinates (r,z) assuming axial symmetry of the time varying components $(\partial/\partial\theta = 0)$. The RF coil is simulated by a perfect conductor of cylindrical shape and rectangular cross section carrying a uniform current density. The approximation of the 6 turn solenoid by a perfect conductor implies that the resistive voltage drop across the solenoid turns cannot be taken into account. Therefore a purely inductive coupling with the plasma is simulated, excluding the capacitive contribution to the discharge. The simulation volume is uniformly subdivided in square cells in (r,z). The plasma current at the grid points is obtained by linear interpolation of the electron and ion current. The following boundary conditions are employed for Eqs. (1), (2) at each boundary: i) $E_\theta = 0$ at $r = 0$, ii) the radiation boundary condition by Bayliss and Turkel at $r = r_{max}$ [6], and iii) the Mur absorbing boundary condition at the boundary $z = z_{min}$ and $z = z_{max}$ [7].

3D3V Particle dynamics - Motion of particles in the electromagnetic field is described by the following equation:

$$m_k \frac{d\mathbf{v}_k}{dt} = q_k(\mathbf{E} + \mathbf{v} \times \mathbf{B} + collisions) \quad k = \text{ion, electron} \tag{3}$$

where m_k, v_k and q_k are respectively the particle mass, velocity and charge. Particle motion and the resulting plasma current, which is the sum of the electron and the ion contribution ($\mathbf{j}_{plasma} = \mathbf{j}_e + \mathbf{j}_i$), are solved in a 3D domain (r,θ,z) by the Boris-Buneman version of the leap-frog method [8]. The plasma current is then averaged in the θ-direction for the 2D electromagnetic calculation. The electric and magnetic fields at the electron/ion position are interpolated from the values at the four neighbour grid points. Trajectories of secondary electrons produced by ionization are also tracked while particles reaching the plasma chamber are lost on the wall and removed from the computation. Collisions are taken into account by the Monte Carlo method where electron collisions with hydrogen atoms, molecules and ions are modelled by the Null-Collision method [9]. In the present model electron-electron and ion-ion collisions are not taken into account, but need to be considered in future studies. A summary of the main collision processes are given in Tab. 1.

TABLE 1. Main collisions in Hydrogen plasma

Collision Type	Before	After	Reference
Elastic	$e^- + H$	$e^- + H$	[11]
	$e^- + H_2$	$e^- + H_2$	[12]
Ionization	$e_1^- + H(1s)$	$e_1^- + H^+ + e_2^-$	[13]
	$e_1^- + H_2(X^1\Sigma_g^+)$	$e_1^- + H_2^+(v) + e_2^-$	[13]
Dissociative ionization	$e_1^- + H_2(X^1\Sigma_g^+)$	$e_1^- + H^+ + H(1s) + e_2^-$	[13]
	$e_1^- + H_2^+$	$e_1^- + H^+ + H^+ + e_2^-$	[13]
Dissociation	$e^- + H_2(X^1\Sigma_g^+)$	$e^- + H(1s) + H(1s)$	[13]

4. MODEL GEOMETRY AND SIMULATION PARAMETERS

A sketch of the simulation geometry is shown in Fig. 2. The plasma chamber has a radius of 24 mm and an overall length of 136 mm. The RF coil has an internal radius of 30 mm and rectangular cross section of dimensions 26x2 mm. The dimensions of the FDTD domain are taken to be double of the plasma chamber in order to avoid large reflections at the boundary. The volume is subdivided uniformly in square cells of 2 mm side. A time step of 1 ps is chosen, in order to remain below the cyclotron period for electrons. Collisions are evaluated at a larger step interval, each $\Delta t_{coll} = 1.0 \times 10^{-8}$ s. RF coil parameters are chosen to simulate the Linac4 source operated at 40 kW RF power, 2 MHz frequency, corresponding to an antenna current of 200 A. A field map of $\mathbf{B}_{cusp}$ is imported from another source. Initially 20000 macro-particles (10000 electrons and 10000 ions) with specific weight of $1{\cdot}10^5$ (ratio of real particles per macro-particle) are uniformly distributed in the region $0 \leq r \leq 12$ mm and $0 \leq z \leq 136$ mm. This results in an initial electron and ion density of $4{\cdot}10^{12}$ m^{-3}. A 300 K Maxwellian initial distribution is assumed. A summary of the input parameters to the simulation can be found in Table 2.

TABLE 2. Simulation input parameters

Initial particle number	20000	H_2 gas pressure	0.03 mbar
Specific weight	10^5	H_2 temperature	300 K
RF frequency	2 MHz	Initial electron temperature	300 K
Coil peak current	200 A	Time step Δt	10^{-12} s
Cell size	2x2 mm	Collision time step Δt_{coll}	10^{-8} s

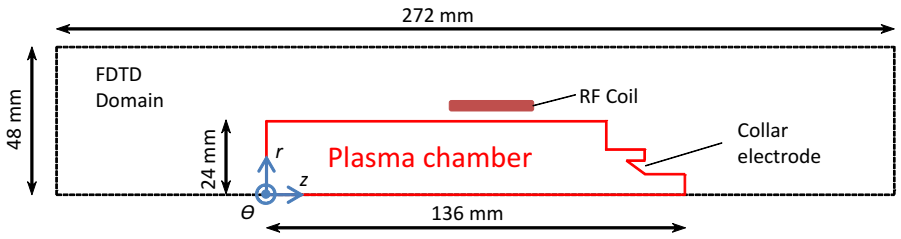

FIGURE 2. Inner volume of the plasma chamber with expansion region and Finite Difference Time Domain. The origin of the right-handed cylindrical coordinates basis is indicated

5. SIMULATION RESULTS

Simulations of the Linac4 ion source were performed on a single computer (2 GHz dual core vPro cpu and 8 GB RAM). Starting from a uniform initial distribution of 20000 particles, we performed simulations of 1.5 μs, which required approximately 18 hours of computational time. We have calculated the plasma time evolution in two configurations, with and without the effect of $\mathbf{B}_{cusp}$. In the latter, the 3D profile of $\mathbf{B}_{cusp}$ is calculated prior to the simulation and used in Eq. (3) in addition to $\mathbf{B}_{RF}$.

Electron density - Average electron density (number of electrons divided by the entire plasma chamber volume) is presented in Fig. 3 as a function of time. During the first 0.5 μs the electron density is generally decreasing. After this time an increase for the whole simulation time (1.5 μs) is observed, with a sharper rise in the case without $\mathbf{B}_{cusp}$. During each RF cycle (500 ns), an increase of the electron density is followed by a sharp decrease. This trend is clearly more marked in absence of $\mathbf{B}_{cusp}$.

Steady RF plasma conditions can only be reached when ionization and losses balance each other during an RF cycle. In our simulation the continuous increase of the electron density over time implies that stable conditions are not reached within the simulation time (1.5 μs) and therefore our time scale is only representative of a discharge initiation in which the electron density is building up. The initial decrease can be ascribed to the artificial initial distribution, which causes wall losses in the first cycle. The slow increase followed by sharp decrease over one RF cycle can be clearly understood by looking at the gas ionization and wall losses.

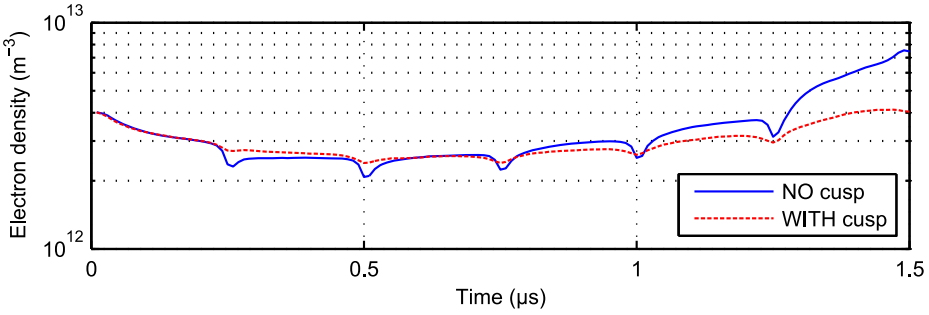

FIGURE 3. Electron density as a function of time with and without $\mathbf{B}_{cusp}$

Gas ionization - Gas ionization (number of macro particles produced by ionizing electron impact with neutral Hydrogen) and wall losses (number of macro particles lost at the wall) are plotted in Fig. 4 as a function of time, together with the electric and magnetic field. Both gas ionization and wall losses present sharp peaks at specific times, specifically every 250 ns, corresponding to half the cycle time. Radial losses are maximum when $B = 0$ and the gas ionization presents a steep increase for $E = E_{max}$. Except from the first half cycle, the radial losses are the dominant loss mechanism.

During an RF cycle $\mathbf{B}_{RF}$ is directly proportional to the coil current. As $\mathbf{B}_{RF}$ increases from zero to maximum, the charged particles (electrons and ions) experience a stronger magnetic field which results in plasma confinement to the center of the chamber. On the other hand when $\mathbf{B}_{RF}$ inverts, there is a de-confinement effect. Gas ionization, con-

versely, depends on the induced electric field, which has a 90 degrees phase difference with respect to the B-field. As the E-field increases, electrons are accelerated in the azimuthal direction, eventually reaching the threshold energy to cause ionization (13.6 eV for H and 15.4 eV for H_2).

When $\mathbf{B}_{cusp}$ is applied, the charged particles experience a constant radial confinement effect. The radial wall losses are greatly reduced in such configuration as indicated in Fig. 5a. However, a drop in the ionization is also observed (Fig. 5b).

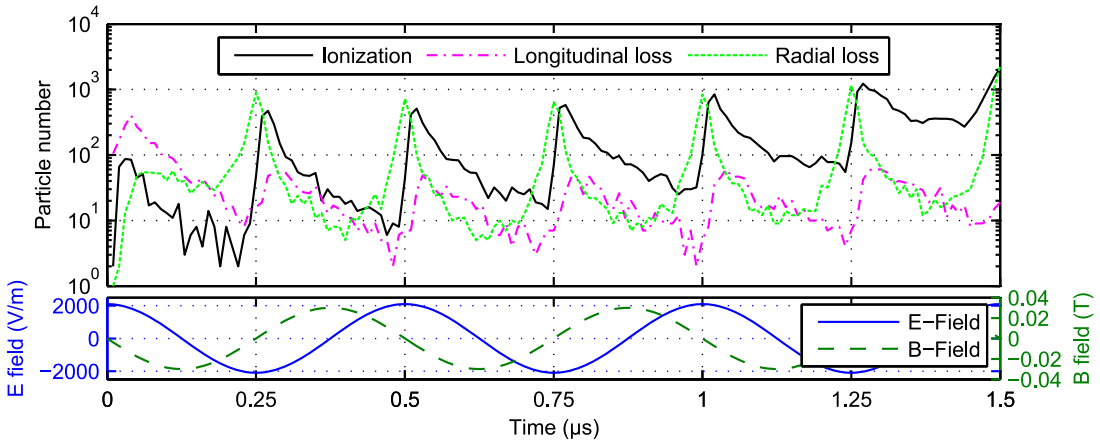

FIGURE 4. Ionization vs. wall losses as a function of time (top) without $\mathbf{B}_{cusp}$. **E** and **B** field (bottom) evaluated at $r = 12, z = 78$ mm (half of the plasma chamber radius and coil center in z direction)

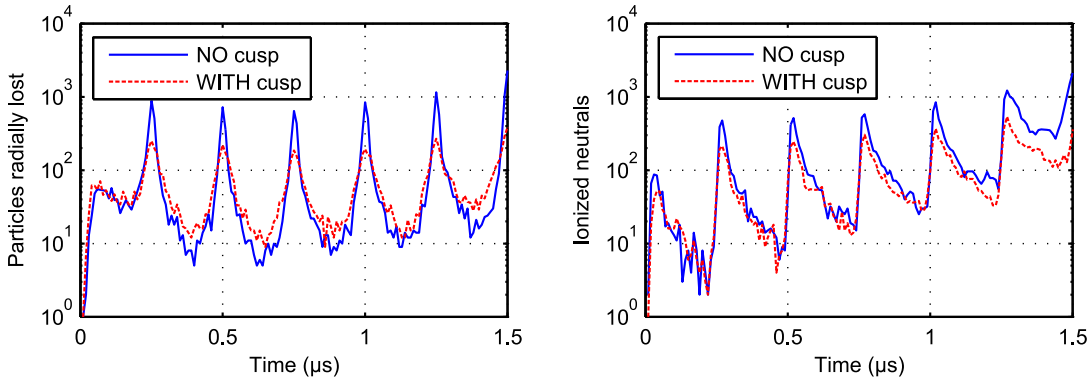

(a) (b)

FIGURE 5. Radial losses (a) and gas ionization (b) as a function of time, with and without $\mathbf{B}_{cusp}$

Joule heating power and electron energy - The heating efficiency can be described by the Joule heating power, which is the product of the electric field and the plasma current. 2D plots of the Joule heating power density (power per cell area) and its average over the radial direction are presented in Fig. 6. The power deposition is higher in magnitude in the absence of $\mathbf{B}_{cusp}$ and its spatial distribution extends radially for the whole plasma chamber. In contrast the application of $\mathbf{B}_{cusp}$ attenuates the power deposition in the region close to the wall, where $\mathbf{B}_{cusp}$ is the strongest.

The discrepancy arises in a different amplitude of the plasma current as a function of the radius as indicated in Fig. 7a, which sharply falls to zero in the 8 mm radius close to

the wall. The electric field is the same in the two configurations and has no contribution to the different behaviour.

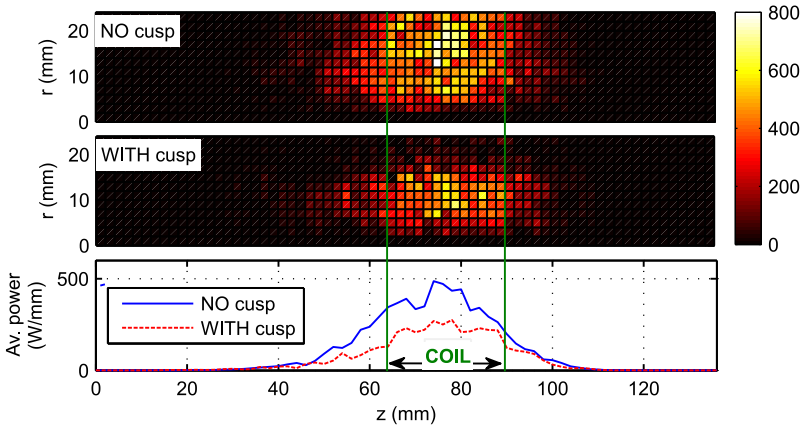

FIGURE 6. 2D Joule heating power densities (W/mm^2) and corresponding average in the radial direction, evaluated at t=1μs (time of maximum E-field)

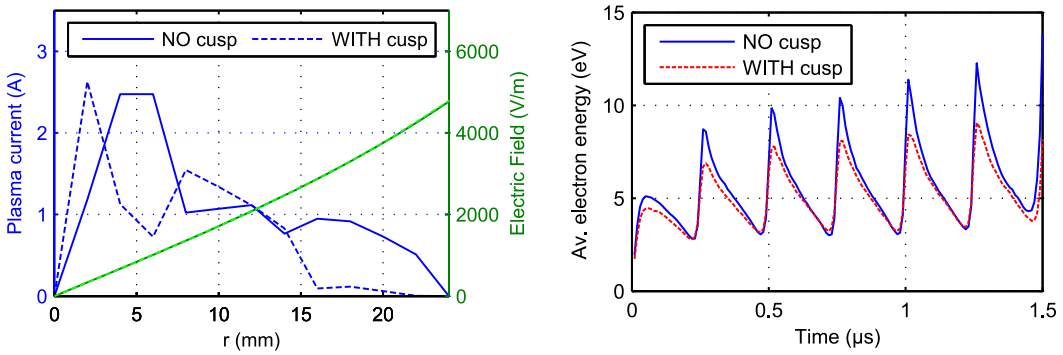

FIGURE 7. Plasma current and electric field as a function of the radius at t=1μs (a). Evolution of the average electron energy in time (b)

The reduced heating efficiency can be ascribed to the reduced mobility of the electrons in the region close to the wall, under the effect of $\mathbf{B}_{cusp}$. Since the electrons in this area are magnetized, the electric field can no longer constantly accelerate them in the azimuthal direction, reducing therefore the plasma current, and therefore the power deposition. The higher Joule heating power deposited in the plasma without $\mathbf{B}_{cusp}$ results in a higher electron energy (Fig. 7b). This, in turn, produces a higher ionization and results in a faster increase of the electron density over time.

6. CONCLUSION AND OUTLOOK

A simplified model of the Linac4 ion source plasma generator was simulated. We have analysed an RF plasma discharge initiation in the low plasma density regime, taking into account the effect of $\mathbf{B}_{cusp}$. Simulations show that although $\mathbf{B}_{cusp}$ limits the radial

losses, a reduced electron energy and gas ionization result in this configuration. The effect is due to the reduced mobility of electrons close to the wall under the effect of $\mathbf{B}_{cusp}$. This prevents their continuous acceleration in the azimuthal direction during the positive phase of the RF electric field.

The stand-alone implementation of the code limited us to 1.5 μs time and densities in the order of 10^{12}-10^{13} m^{-3}. To simulate the Linac4 ion source plasma densities of 10^{19} m^{-3} a major upgrade is needed. The development of a parallelized code, exploiting the symmetries of the source to reduce the computational domain is foreseen.

Analysis of the Joule heating power indicated that the RF plasma heating only takes place in the central region of the plasma chamber. Reduction of the computational domain to this relevant region, if implemented, needs to be followed by an analysis of the plasma expansion towards the extraction region. Particle fluxes with the respective energies will then be transferred to a separate code specific for the extraction physics.

In the presented initial analysis for Linac4, H^- production processes have not yet been included for simplicity, as shown in Table 1. These H^- processes, however, are very important for the simulation and will be included in the future. The H atom and H_2 molecule transport modeling will also be important for the understanding of the H^- production processes. 3D modeling of Maxwell Eqs. (1), (2) will be needed to take into account the full 3D dynamics of the plasma particles and the resultant plasma current $j_{plasma}(r,\theta,z)$ obtained by Eq. (3). This will also allow to take into account the real geometry of the antenna and the capacitive coupling between the RF-coil and the plasma.

ACKNOWLEDGMENTS

The authors thank M. Eng. S. Yoshinari (present address: Nihon Unisys) and M. Eng. T. Hayami (present address: Nomura Research Institute) for their extensive efforts to develop the EM-PIC-MCC code. Furthermore, we are grateful to Eric McIntosh for his considerable support in setting up the code at CERN.

REFERENCES

1. M. Vretenar, et al., *CERN-ATS-2011-041* (2011).
2. J. Lettry, et al., "H^- ion sources for CERN's Linac4," in *These proceedings*, 2012.
3. S. Yoshinari, T. Hayami, R. Terasaki, A. Hatayama, and A. Fukano, *Review of Scientific Instruments* **81**, 02A728 (2010).
4. T. Hayami, S. Yoshinari, R. Terasaki, A. Hatayama, and A. Fukano, "Analysis of Discharge Initiation in a RF Hydrogen Negative Ion Source," in *American Institute of Physics Conference Series*, 2011.
5. K. Yee, *Antennas and Propagation, IEEE Transactions on* **14**, 302–307 (1966), ISSN 0018-926X.
6. A. Bayliss, and E. Turkel, *Communications on Pure and Applied Mathematics* **33** (1980).
7. G. Mur, *Electromagnetic Compatibility, IEEE Transactions on* **EMC-23**, 377–382 (1981).
8. C. Birdsall, and A. Langdon, *Plasma Physics via Computer Simulation*, 2004.
9. K. Nanbu, *Plasma Science, IEEE Transactions on* **28**, 971–990 (2000).
10. *Journal of Computational Physics* **25**, 205 – 219 (1977).
11. S. Buckman, et al., *Interactions of Photons and Electrons with Atoms*, Springer-Verlag, 2000.
12. S. Buckman, et al., *Interactions of Photons and Electrons with Molecules*, Springer-Verlag, 2003.
13. R. Janev, *Elementary processes in hydrogen-helium plasmas: cross sections and reaction rate coefficients*, Springer-Verlag, 1987.